

High-performance photorefractive organic glasses: understanding mechanisms and limitations

¹O.Ostroverkhova, ^{1*}U. Gubler, ^{1**}D. Wright, ²M. He, ²R.J.Twieg, ¹W.E. Moerner

¹Department of Chemistry, Stanford University, Stanford, CA 94305-5080

²Department of Chemistry, Kent State University, Kent, OH 44242-0001

ABSTRACT

Since the first observation of the photorefractive (PR) effect in polymers, extensive efforts have been directed toward understanding the physics of the PR process in these systems, as well as optimizing polymer composites and glasses for various applications. Despite remarkable progress both in elucidating the mechanisms and processes contributing to the PR effect and in designing organic materials with high gain and diffraction efficiency, simultaneously attaining high refractive index modulation, fast dynamics, and good thermal properties in one material remains a challenge. Monolithic glasses represent an attractive class of PR organic materials since they possess large nonlinearities and minimal inert volume, which enhances the performance without stability problems. In this paper, we present a complete study of monolithic glasses based on a promising new class of chromophores (containing 2-dicyanomethylen-3-cyano-5,5-dimethyl-2,5-dihydrofuran, abbreviated as DCDHF-derivatives). We describe thermal, photoconductive, orientational, and photorefractive properties of these materials in both red and near infrared wavelength regions. By studying the temperature dependence of various parameters, we analyze the factors that affect photorefractivity in DCDHF-based materials.

Keywords: photorefractive organic materials, monolithic glasses

1. INTRODUCTION

The photorefractive (PR) effect is a dynamic refractive index change induced by nonuniform illumination via a space-charge electric field formation and the electro-optic nonlinearity.^[1] Materials in which the PR effect is observed, or PR materials, are of interest due to potential holographic applications in optical data storage, optical computing, image processing, phase conjugation and many others.^[2,3] In particular, PR organic materials are technologically attractive due to their low cost, ease of fabrication and chemical tunability.^[4]

The PR effect in organic materials comprises various processes such as charge photogeneration, transport, and trapping that contribute to a space-charge field formation, with a subsequent re-orientation of the nonlinear optical chromophores in the space-charge field.^[4] Due to the complex nature of the effect, the design of an “ideal” photorefractive material with good steady-state and dynamic PR performance as well as good thermal properties represents a challenge. The reason is that characteristics of materials that are beneficial for the steady-state performance could be detrimental for both the PR dynamics and thermal stability. For example, materials possessing high dipole moments and containing high trap densities are required for the best steady-state performance. However, these properties lead to slower PR dynamics due to the decreased charge carrier mobility arising from the increase in disorder.^[5] Also, strong dipole-dipole interactions lead to a variety of instabilities, in particular, dye aggregation,^[6] crystallization, and phase separation,^[7,8] which shortens the material shelf life and, therefore, makes the material unsuitable for applications. For example, it is known that a high concentration of the nonlinear optical chromophore is required to produce large refractive index modulations. In polymer composites, this may lead to phase separation and crystallization, which compromises the optical quality and, therefore, device performance and durability. In contrast, monolithic glasses possess large nonlinearities without stability problems due to phase separation. Also, incorporating all the functionality into a single component minimizes inert volume which otherwise limits the change in refractive index that can be achieved. Similarly, for facile charge transport via hopping, the transporting molecules should also be present in high volume

* Present address: CSEM Alpnach, Switzerland

** Present address: Ecole Normale Supérieure de Cachan, Paris, France

fraction. Simultaneously maximizing the volume allotted to transport and the volume allotted to nonlinearity is easily achieved with a monolithic glass based on a multifunctional molecule.

Previously, our group reported a new nonlinear optical chromophore 2-dicyanomethylen-3-cyano-5,5-dimethyl-4-(4'-dihexylaminophenyl)-2,5-dihydrofuran (abbreviated as DCDHF-6, see below), which, when incorporated into a PVK/BBP/C₆₀ composite, exhibited high two-beam coupling gain coefficients of 400 cm⁻¹ and sub-second response times at applied electric fields of 100 V/μm.^[9] Differential scanning calorimetry (DSC) analysis showed that even the neat DCDHF-6 chromophore can form an amorphous organic glass.^[10] High gain coefficients of ~150 cm⁻¹ at an applied field of only 25 V/μm observed in DCDHF-6 – based photorefractive glasses^[10] prompted us to extend our exploration to a number of additional DCDHF derivatives.^[11] In this paper, we present our study of several photorefractive organic glasses based on DCDHF. We analyze both steady-state and dynamical photorefractive performance of these glasses at a wavelength of λ=676 nm when sensitized with C₆₀ and at λ=830 nm when sensitized with (2,4,7-trinitro-9-fluorenylidene)malonitrile (TNFM). Photoconductivity, birefringence, and chromophore re-orientational mobility, as well as their contribution to the photorefractive speed are discussed. By studying the temperature dependence of various parameters, we relate the orientational and PR dynamical properties as well as investigate the nature of shallow traps.

2. EXPERIMENTAL

2.1 Materials

The DCDHF derivatives used in this study are shown in Figure 1.

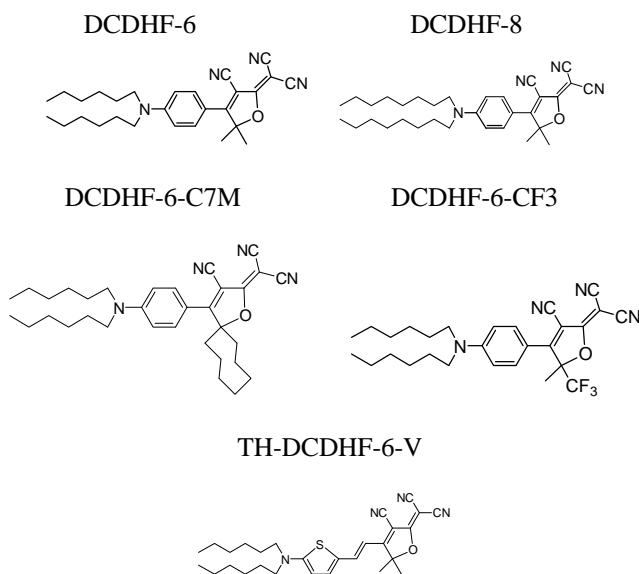


Figure 1. Molecular structures of DCDHF-based chromophores used in photorefractive studies.

Most of the molecules shown in Figure 1, except for TH-DCDHF-6-V, formed a glassy state at room temperature. In addition, mixtures of several DCDHF molecules also formed glass. Detailed study of thermal properties of DCDHF derivatives and their mixtures can be found in the accompanying paper.^[12] Here, we only summarize the thermal properties of the compounds used in our photorefractive experiments (Table 1).

Compound number	Description	T _g , °C; stability of glassy state
1	DCDHF-6	19; unstable
2	DCDHF-6-C7M	33; unstable
3	DCDHF-8	1; unstable
4	DCDHF-6-CF3	17; stable
Mix 5	TH-DCDHF-6-V/DCDHF-8 (1:1 wt)	22; unstable
Mix 6	DCDHF-6/DCDHF-6-C7M (1:1 wt)	23; stable
Mix 7	DCDHF-8/DCDHF-6-C7M (1:1 wt)	20; stable

Table 1. Thermal properties of several DCDHF-containing photorefractive materials.

2.2 Sample preparation

The samples contained 99.5 wt. % DCDHF chromophore and 0.5 wt.% C₆₀ or TNFM depending on the wavelength region being assessed. The DCDHF chromophores and C₆₀ or TNFM were dissolved in chlorobenzene (50 mg/ml in the case of DCDHF and 1 mg/ml in the case of C₆₀ and TNFM), stirred, filtered through a 0.2 μm filter and cast on ITO-coated glass slides. The films were dried overnight in an oven at 120 °C. When the residual solvent evaporated, the ITO slides with films were heated up to a temperature slightly higher than the melting point of the chromophore (125-140 °C), sandwiched with 70-90 μm spacers and quenched by placing the sample on a metal plate at room temperature. With some of the chromophores, fast cooling is crucial since otherwise the material crystallizes instead of forming a glass. Such glasses are thermodynamically unstable (Table 1) and re-crystallize during the period of 2-8 weeks, depending on the material. The stable glasses maintained good optical quality over the period of at least eight months so far.

2.3 Optical properties

The optical properties of various DCDHF derivatives are described in detail in the accompanying paper.^[12] Here, the absorption spectra of only a few DCDHF chromophores, relevant for our photorefractive studies, are discussed. Absorption spectra of dilute solutions of DCDHF-6, DCDHF-6-CF3 and TH-DCDHF-6-V chromophores in THF are shown in Figure 2.

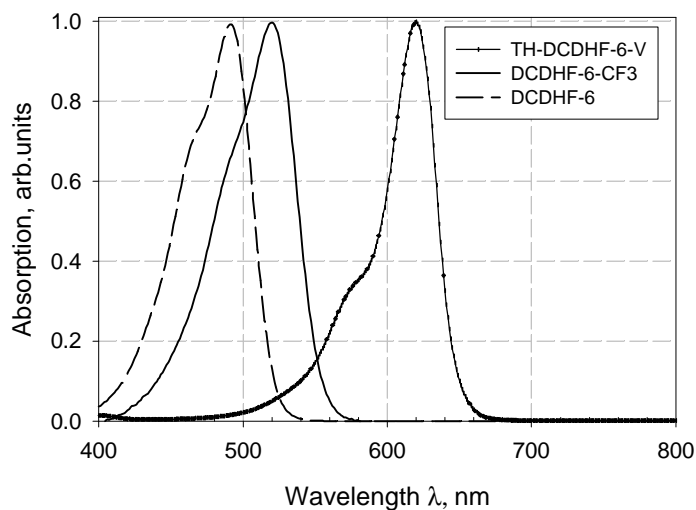


Figure 2. Absorption spectra of selected DCDHF chromophores in THF (normalized).

The absorption spectra of DCDHF-8 and DCDHF-6-C7M (not shown) are similar to that of DCDHF-6. As seen in Figure 2, all the chromophores possess low absorption at a wavelength of 830 nm, and most of them (except for TH-DCDHF-6-V) possess low absorption at a wavelength of 676 nm, which permits photorefractive studies of the monolithic DCDHF glasses at these wavelengths.

The absorption coefficients (α) of the sensitized DCDHF-based PR films (Section 2.2) were calculated from the absorption spectra using the relation $\mathbf{a} = \frac{A}{L} \ln 10$, where A is the decadic absorbance and L is the sample thickness. At

a wavelength of 676 nm, the absorption coefficients α_{676} of compounds **1-4**, **mix 6**, and **mix 7** sensitized with C_{60} were ~ 10 - 20 cm^{-1} and reflected the absorption of C_{60} . At a wavelength of 830 nm, the absorption coefficients α_{830} of compounds **1-4**, **mix 6**, and **mix 7** sensitized with TNFM were due to the sensitizer and below 10 cm^{-1} , while in **mix 5**/TNFM, higher absorption coefficients of $\sim 80 \text{ cm}^{-1}$ were observed due to both the sensitizer and TH-DCDHF-6-V chromophore absorption.

2.4 DC conductivity

DC conductivity measurements were conducted at a wavelength of 676 nm (Kr^+ laser). The electric field was applied to the sample, and the dark current (i_d) was monitored with a current amplifier and a computer. Then, the laser beam was allowed to hit the sample with a shutter, and a current in the presence of light (i_l) was monitored. The photocurrent was obtained as a difference between i_l and i_d : $i_{ph} = i_l - i_d$. The dark (\mathbf{S}_d) and photoconductivity (\mathbf{S}_{ph}) were calculated using $\mathbf{S}_{d,ph} = i_{d,ph} / (SL)$, where S is the electrode sample area, and L is the sample thickness.

2.5 Electric field-induced birefringence

Electric field-induced birefringence was measured using a conventional transient ellipsometry technique. Light of wavelength $\lambda=976 \text{ nm}$ (laser diode) was polarized at 45° with respect to the plane of incidence. The sample was placed between crossed polarizers at an angle of 54° between the sample normal and the light beam. The residual sample birefringence was compensated by a Soleil-Babinet compensator, so that no transmitted light could be detected in the absence of electric field. The electric field was applied to the sample as a step function with a rise time below $100 \mu\text{s}$, and the intensity of transmitted light was recorded as a function of time. Then, the electric field was turned off, and the decay of the transmitted light intensity (I) was monitored. The birefringence was calculated using the formula

$$\Delta n = \frac{I \cos \mathbf{j}}{2pd \sin^2 \mathbf{j}} \arcsin \sqrt{I/I_{\max}},$$

where λ is wavelength, φ is the internal incident angle, d is the sample thickness, and I_{\max} is the maximal transmitted intensity.

2.6 Photorefractive experiments

Two-wave mixing experiments were conducted at wavelengths of 676 nm (Kr^+ laser) and 830 nm (laser diode). The p-polarized beams were incident at external angles of 30° and 60° to the sample normal and the beam intensity ratio was 1:1. The total writing beam intensity was 100 mW/cm^2 . The electric field was applied so that the negative high voltage would be on the sample electrode facing the incident beams. Such an experimental configuration is needed to minimize beam fanning and its related unphysical gain coefficients. The beams were controlled with a magnetic shutter (switching time below $150 \mu\text{s}$), and the intensity of both amplified and depleted beams was monitored. After the measurements, the grating was erased by a larger diameter non-Bragg-matched erasing beam. The gain coefficient Γ was calculated using the formula

$$\Gamma = \frac{\cos \theta_1}{L} \ln \frac{\gamma}{2 - \gamma},$$

where θ_1 is the smaller internal angle of incidence, L is the sample thickness, and $\gamma = I_{\text{with pump}} / I_{\text{without pump}}$.

Four-wave mixing experiments were conducted at $\lambda=676$ nm (Kr^+ laser). The grating was written by two s-polarized beams incident at external angles of 30° and 60° to the sample normal and with beam intensity ratio 1:1. The probe beam was p-polarized, had intensity on the order of 1% of the total writing beam intensity, and was counterpropagating with one of the writing beams. The electric field was applied to the sample, the writing beams were opened with a magnetic shutter, and the diffracted beam was monitored as a function of time. When the diffracted signal reached a steady state, the writing beams were turned off, and either the dark decay or grating erasure in the presence of the erasing beam was recorded. The external diffraction efficiency (η) was calculated as a ratio of the diffracted (I_d) and incident (I_0) probe beam intensities: $h = I_d / I_0$.

3. RESULTS AND DISCUSSION

3.1 Photoconductive properties

The DC photoconductivity of several DCDHF glasses sensitized with C_{60} as a function of light intensity at a wavelength of 676 nm and an electric field of 20 V/ μm is shown in Figure 3.

DCDHF glasses exhibit high photoconductivity of ~ 1 pS/cm at a light intensity of 20 mW/cm^2 and an electric field of 20 V/ μm , which is similar to the photoconductivity values observed in photoconducting polymers such as PVK under similar conditions. The inset of Figure 3 shows a power law fit ($S_{ph} \sim I^a$) to the intensity-dependent photoconductivity for the compound **mix7/C₆₀**. A linear intensity dependence of the photoconductivity is observed in this compound as well as all other DCDHF glasses studied. Further comparative studies of the photoconductivity of various DCDHF glasses can be found in Ref.^[11].

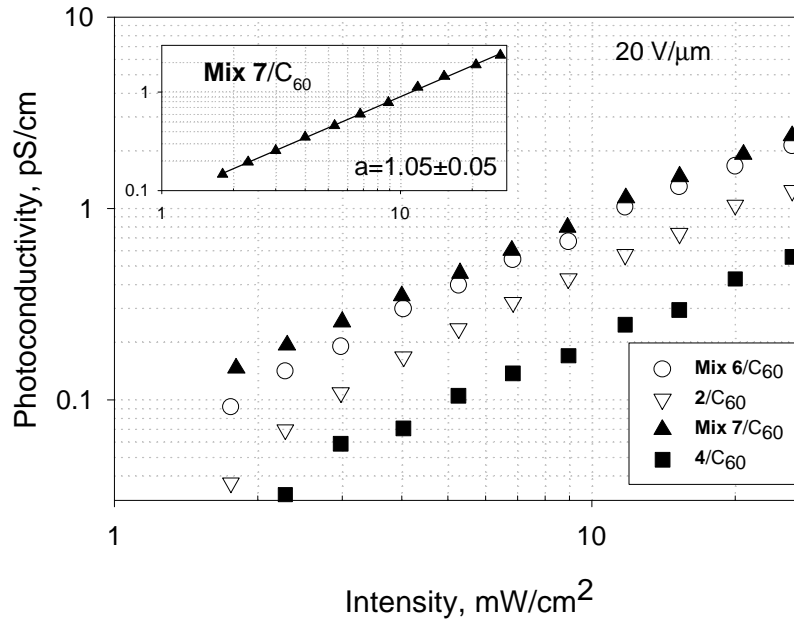


Figure 3. Photoconductivity of DCDHF glasses sensitized with C_{60} . Inset shows a power law fit ($S_{ph} \sim I^a$) to the light intensity dependence of the photoconductivity in compound **mix 7/C₆₀**.

The dark conductivity of DCDHF glasses at temperatures below and around T_g was less than 0.1 pS/cm at 20 V/ μ m. However, increasing the temperature above T_g leads to a strong increase in dark conductivity. The temperature dependence of various parameters, including dark and photoconductivity, in DCDHF glasses will be reported elsewhere.

3.2 Orientational properties

The electro-optic nonlinearity of our glasses as well as the ability of the chromophores to reorient in the electric field was evaluated in the electric field-induced birefringence experiment (Section 2.5). The steady-state birefringence

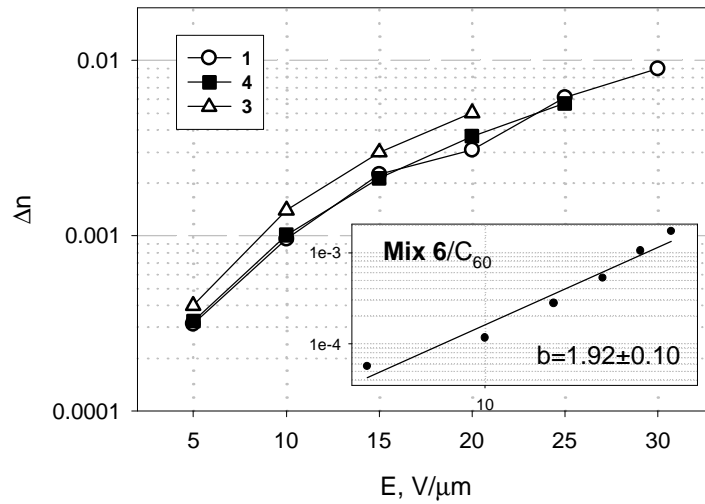


Figure 4. Steady-state birefringence of several DCDHF glasses as a function of electric field.

Inset shows a (log-log) power law fit ($\Delta n \sim E^b$) in the compound **mix 6/C₆₀**.

achieved in compounds **1-3** as a function of applied electric field is shown in Figure 4. High birefringence values, reaching 0.01 at an electric field of 30 V/ μ m, are observed.

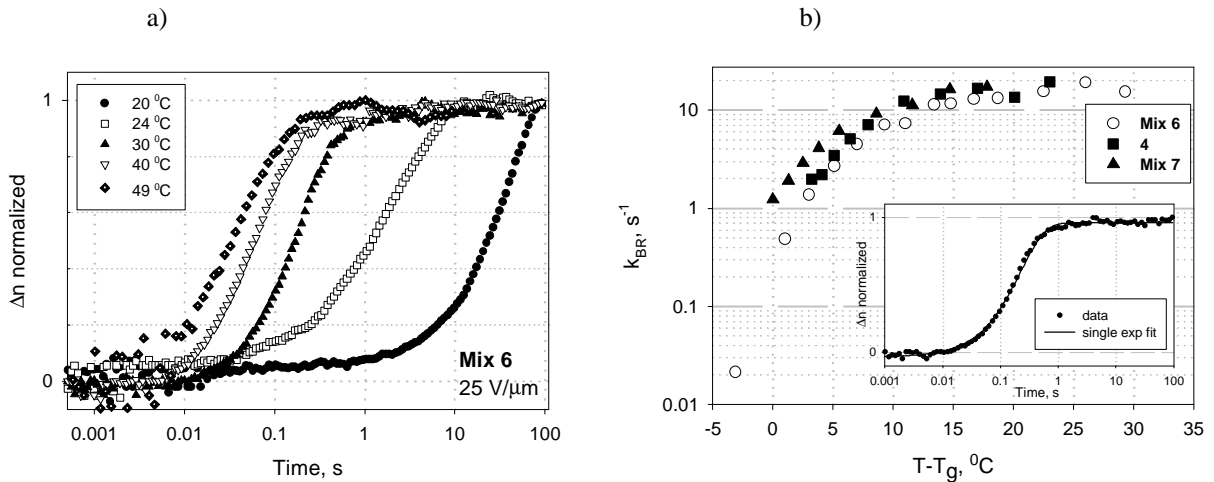


Figure 5. a) Birefringence rise at various temperatures in **mix 6/C₆₀**; b) Orientational speed obtained in several DCDHF compounds as a function of temperature relative to T_g . Inset shows a fit to the transient obtained at 30 °C in **mix 6**.

The inset of Figure 4 shows a power law fit ($\Delta n \sim E^b$) obtained in the compound **mix 6**/ C_{60} . The power law exponent b is close to 2 as expected in the case of low electric fields ($\mathbf{m}^* \cdot \mathbf{E} \ll kT$, where \mathbf{m}^* is the dressed molecular dipole moment, k is Boltzmann's constant, and T is the temperature).^[13]

To investigate the influence of thermal properties of the glasses, in particular glass transition temperature, on the chromophore orientational properties, we performed temperature dependent measurements of the electric field-induced birefringence. The birefringence rise in response to a step-function electric field of 25 V/ μm at various temperatures observed in the compound **mix 6**/ C_{60} ($T_g \sim 23^\circ\text{C}$) is shown in Figure 5(a). As the temperature increases, the chromophore orientation becomes faster, with a largest increase in orientational speed at temperatures right around T_g (Figure 5(a)). The transients are fitted with stretched exponential function ($\Delta n \sim 1 - \exp[-k_{BR}t]^b$) at temperatures below T_g and with single exponential function ($\Delta n \sim 1 - \exp[-k_{BR}t]$) at temperatures above T_g . The inset of Figure 5(b) shows a single exponential fit to the transient obtained at a temperature of 30°C at an electric field of 25 V/ μm in the compound **mix 6**. The orientational speed (k_{BR}) of all DCDHF glasses strongly depends on the temperature relative to T_g as shown in Figure 5(b) for compounds **4**, **mix 6** and **mix 7**. At temperatures several degrees below T_g , the orientational speed is $\sim 0.02 \text{ s}^{-1}$. Increasing the temperature by only 10°C above T_g increases the orientational speed by at least an order of magnitude. At temperatures $\sim 10^\circ\text{C}$ above T_g , the orientational speed is $\sim 10 \text{ s}^{-1}$ for all chromophores, and further increase in temperature leads to a much smaller change in orientational speed in comparison with that in the temperature region around T_g .

3.3 Photorefractive properties

3.3.1 Two-beam coupling

676 nm

Two-beam coupling gain coefficients obtained in compounds **1**, **4**, and **mix 6** sensitized with C_{60} at a wavelength of 676 nm as a function of electric field are shown in Figure 6(a). Absorption coefficients (α_{676}) obtained in these compounds were $\sim 12\text{-}20 \text{ cm}^{-1}$ (dashed lines in Figure 6(a)).

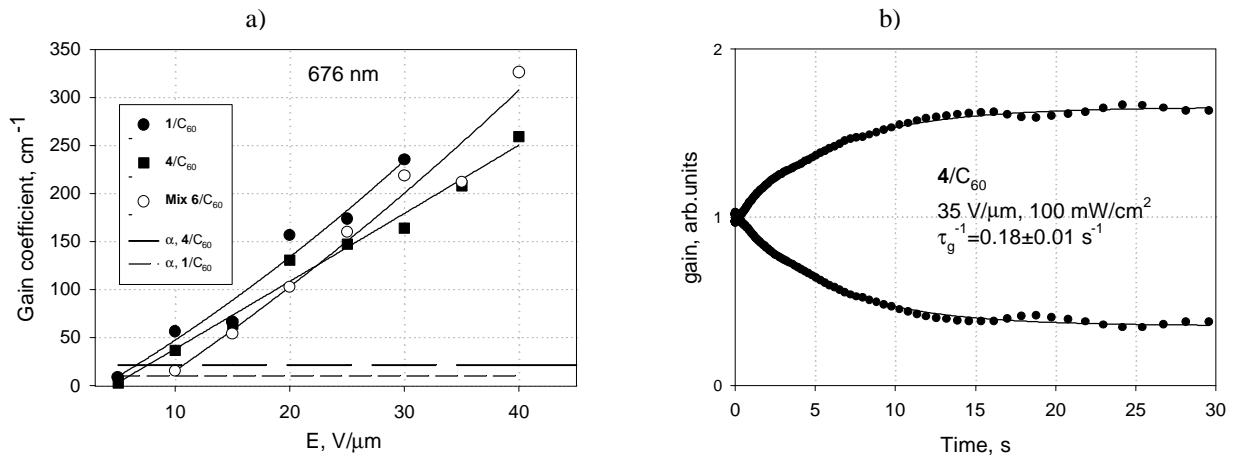


Figure 6. a) Two-beam coupling gain coefficient in DCDHF/ C_{60} glasses at a wavelength of 676 nm as a function of electric field. Solid lines are guides to the eye. Dashed lines correspond to the absorption coefficients; b) Gain versus time obtained in the compound $4/C_{60}$ at an electric field of 35 $\text{V}/\mu\text{m}$ and total writing beam intensity of 100 mW/cm^2 . Solid line shows a single exponential fit to the data.

High gain coefficients (Γ) in combination with low absorption coefficients (\mathbf{a}_{676}) enabled high net gain coefficients ($\Gamma - \mathbf{a}_{676}$) of $\sim 200 \text{ cm}^{-1}$ at electric fields of only 30-40 $\text{V}/\mu\text{m}$. These values are among the highest reported in the literature thus far. A strong beam fanning effect exhibited by DCDHF-containing glasses^[10,11] prevented measurements of the two-beam coupling gain at electric fields higher than 30-40 $\text{V}/\mu\text{m}$.

In many applications, the dynamics of the two-beam coupling effect plays a major role, with fast response a key goal. At temperatures around T_g , the gain dynamics is characterized with a simple single exponential function ($\mathbf{g} \sim 1 - \exp[-\mathbf{t}_g^{-1}t]$ or corresponding decay), in which the parameter τ_g^{-1} describes the PR response speed. Typical data with a single exponential fit is presented in Figure 6(b) for the compound **4**/ C_{60} at an electric field of 35 $\text{V}/\mu\text{m}$ and total writing beam intensity of 100 mW/cm^2 . The fit yielded a PR response time $\tau_g^{-1} \sim 0.18 \text{ s}^{-1}$, which is a typical value for all DCDHF glasses we studied at similar electric fields and relative-to- T_g temperatures. The PR dynamics in DCDHF glasses will be discussed in more detail in Section 3.3.2.

830 nm

Two-beam coupling gain coefficients obtained in compounds **1**, **mix 5** and **mix 6** sensitized with TNFM at a wavelength of 830 nm as a function of electric field are shown in Figure 7(a). The absorption coefficients (\mathbf{a}_{830}) obtained in compounds **1** and **mix 6** /TNFM were below 10 cm^{-1} (dashed line in Figure 7(a) describes the absorption in both compounds), while the absorption coefficient in the compound **mix 5**/TNFM was $\sim 80 \text{ cm}^{-1}$ (dotted line in Figure 7(a)). In spite of the relatively high absorption coefficient in the compound **mix 5**/TNFM, high net gain coefficients of over 200 cm^{-1} at an electric field of 30 $\text{V}/\mu\text{m}$ were achieved in this compound. These are among the highest reported values of gain coefficients observed at near infrared wavelengths at low electric fields. Figure 7(b) shows the gain dynamics observed in the compound **mix 5**/TNFM at an electric field of 45 $\text{V}/\mu\text{m}$. Almost complete energy transfer between the two beams is observed, and similar to the dynamics at a wavelength of 676 nm, the transients can be fitted with a single exponential function ($\mathbf{g} \sim 1 - \exp[-\mathbf{t}_g^{-1}t]$ or corresponding decay), with the PR response speed (\mathbf{t}_g^{-1}) ranging between 0.1 and 0.3 s^{-1} , depending on the electric field, at the total beam intensity of 100 mW/cm^2 .

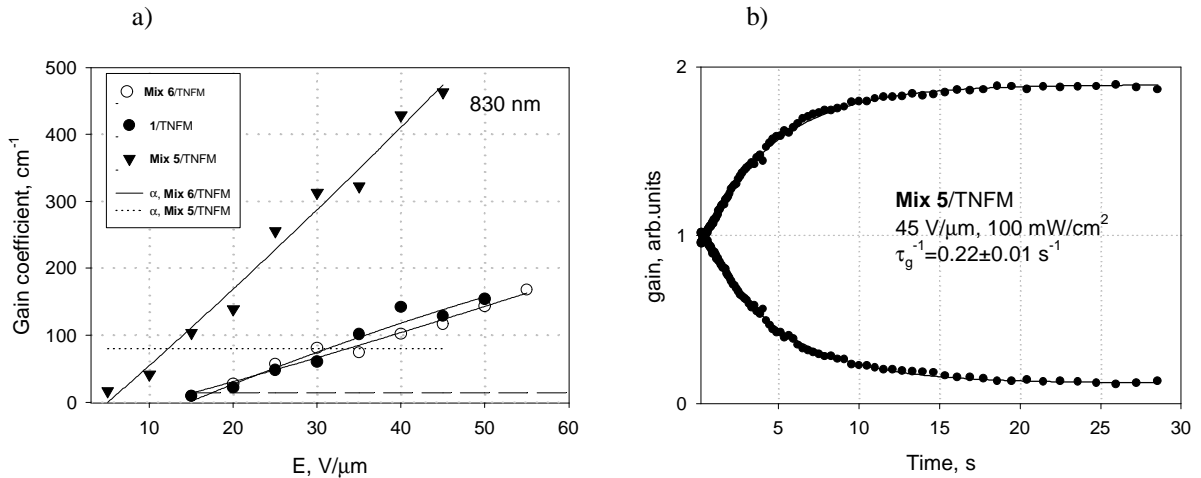


Figure 7. a) Gain coefficient at a wavelength of 830 nm as a function of electric field in several DCDHF/TNFM glasses. Solid lines guide the eye. Dashed and dotted lines represent absorption coefficients in several materials; b) Gain dynamics in **mix 5**/TNFM at an electric field of 45 $\text{V}/\mu\text{m}$ and light intensity of 100 mW/cm^2 . Solid line corresponds to a single exponential fit of the data.

It is well-known that the sensitizer plays a crucial role in the dynamics of PR materials.^[4] Although the role of the sensitizer in the steady-state PR performance is not as clearly defined, several studies confirmed that sensitizer influences the trapping properties of the PR material, essential for space-charge field formation.^[14-16] Our results of two-beam coupling experiments performed at different wavelengths in DCDHF monolithic glasses further confirm this fact. Figures 8(a) and 8(b) show electric field dependence of the gain coefficients obtained in compounds **4** and **mix 6** sensitized with C₆₀ at a wavelength of 676 nm and with TNFM at a wavelength of 830 nm, respectively.

The gain coefficients observed in both glasses at a wavelength of 830 nm are several times smaller than those observed at a wavelength of 676 nm. This difference is far larger than expected due to the change in grating period as the wavelength changes with the angle between the writing beams kept the same.^[17] Moreover, while the similar gain coefficients were obtained in compounds **4**/C₆₀ and **mix 6**/C₆₀ at 676 nm, rather different performance was obtained in

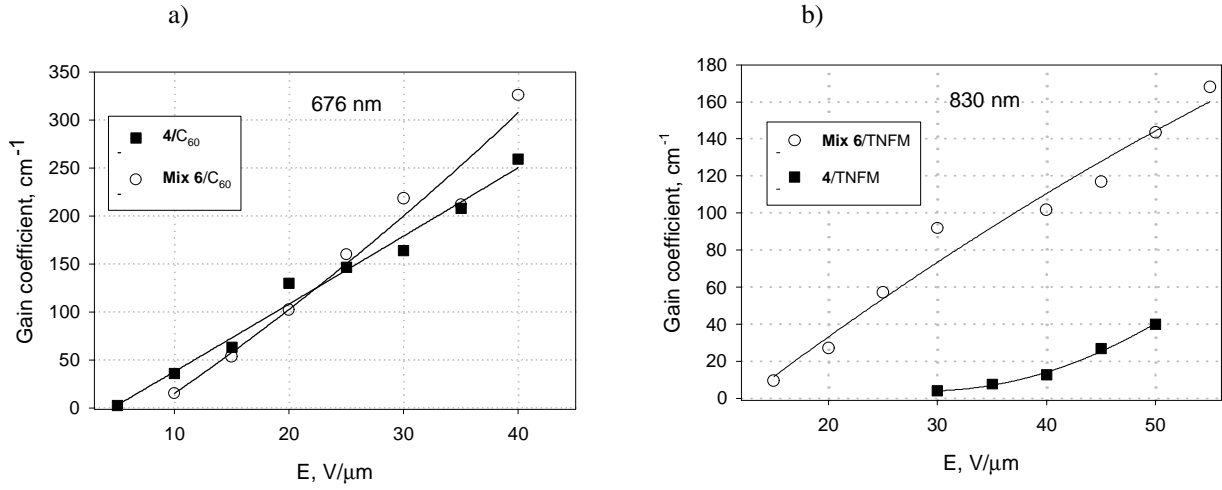


Figure 8. a) Gain coefficient of **4**/C₆₀ and **mix 6**/C₆₀ as a function of electric field at a wavelength of 676 nm; b) Gain coefficient of **4**/TNFM and **mix 6**/TNFM as a function of electric field at a wavelength of 830 nm. Lines guide an eye.

TNFM-sensitized version of the same glasses at 830 nm. This suggests that TNFM is a better sensitizer for the compound **mix 6** than for the compound **4** and underscores the role of the sensitizer in trapping dynamics, which determines the magnitude of the space charge field and, therefore, the gain coefficient.^[14]

3.3.2 Four-wave mixing

The four-wave mixing geometry was used to further study the PR dynamics at a wavelength of 676 nm. The refractive index modulation (Δn_{FWM}) was calculated from the diffraction efficiency,^[4] and the transients due to PR grating formation were fitted with a stretched exponential function ($\Delta n_{FWM} \sim 1 - \exp[-(\mathbf{k}_r t)^b]$) at temperatures below T_g and a single exponential function ($\Delta n_{FWM} \sim 1 - \exp[-\mathbf{k}_r t]$) at temperatures at and above T_g. Figure 9(a) shows the dependence of the PR rise speed (\mathbf{k}_r) on the total writing beam intensity at various temperatures, obtained in the compound **mix 6**/C₆₀ (T_g~23 °C) at an electric field of 20 V/μm. Figure 9(b) shows typical data and a single exponential fit to the refractive index modulation (Δn_{FWM}) time evolution in the same compound at 23 °C. The power law fits ($\mathbf{k}_r \sim I^c$) yield the power exponent $c \sim 0.23$ at a temperature of 21 °C, indicating weak intensity dependence of the PR speed at temperatures below T_g, which is the evidence of orientationally-limited PR behavior. The similarity of the PR speed $\mathbf{k}_r \sim 0.025\text{-}0.045 \text{ s}^{-1}$ and the orientational speed $k_{BR} \sim 0.02 \text{ s}^{-1}$, obtained in the electric-field-induced birefringence

experiment at 21 °C in this compound (see Figure 5(b)), further confirms that at temperatures below T_g , the PR speed observed in DCDHF glasses is limited by the speed of chromophore orientation in the electric field. As the temperature increases above T_g , the orientational speed dramatically increases (Figure 5(b)): a several degree increase above T_g leads

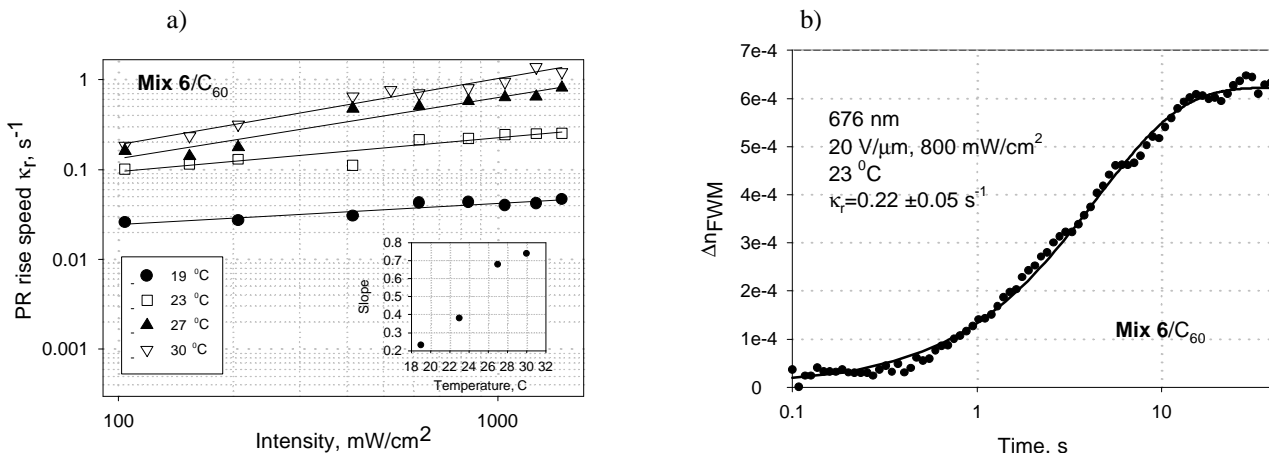


Figure 9. a) PR rise speed of the compound **mix 6/C₆₀** at an electric field of 20 V/μm as a function of light intensity at various temperatures. Solid lines correspond to the power law fits $\kappa_r \sim I^c$. Inset shows the dependence of the power exponent c on temperature; b) Time evolution of refractive index modulation, calculated from diffraction efficiency, in the compound **mix 6/C₆₀** at an electric field of 20 V/μm, light intensity of 800 mW/cm² and temperature of 23 °C. Solid line shows a single exponential fit to the data.

to an order of magnitude increase in the PR speed. Also, the intensity dependence of the PR speed becomes stronger, as the PR speed becomes photoconductivity-limited, and reaches values of $\sim 1\text{--}2$ s⁻¹ at an electric field of 20 V/μm and light intensity of ~ 1 W/cm². The inset of Figure 9(a) demonstrates an increasing power law exponent c as a function of temperature, obtained in the compound **mix 6/C₆₀**.

To probe the nature of shallow traps in DCDHF glasses, we studied PR grating dark decay. The decay of refractive index modulation was fitted with a single exponential function ($\Delta n_{FWM} \sim \exp[-k_d t]$), and the dark decay speed (k_d) was

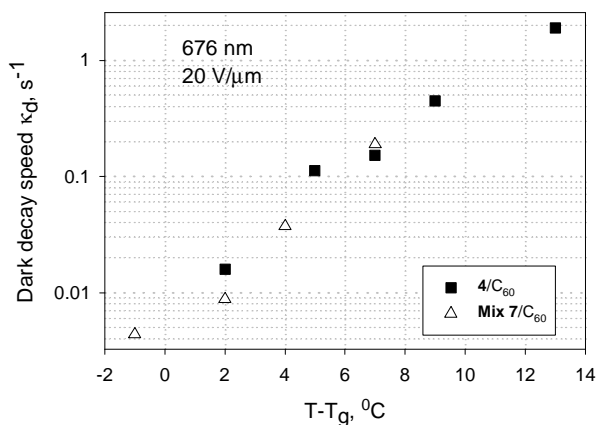


Figure 10. Dark decay speed as a function of temperature relative to T_g , obtained in 4/C₆₀ and **mix 7/C₆₀** compounds at an electric field of 20 V/μm.

measured as a function of temperature for various glasses. The dark decay speed strongly depends on the temperature relative to T_g , as shown in Figure 10 for the compounds 4/C₆₀ and **mix 6/C₆₀**. A temperature increase of ~ 10 °C above T_g

increases the dark decay speed by at least an order of magnitude. Also, the dark decay speed in all compounds studied depends on temperature relative to T_g , rather than on the absolute temperature. A strong T- T_g dependence of the dark decay speed, which is universal for all DCDHF glasses, suggests that the increase in charge release from shallow traps in DCDHF glasses are related to the molecular arrangement in the bulk rather than to chemical impurities. Detailed study of these properties will be reported elsewhere.

4. CONCLUSIONS AND OUTLOOK

In this paper, the photoconductive, orientational, and photorefractive properties of several new DCDHF-based high performance organic glasses have been presented, with emphasis on the changes in these properties that result from temperature changes relative to T_g . High photoconductivities of $\sim 1 \text{ pS/cm}$ at $20 \text{ V}/\mu\text{m}$ and 20 mW/cm^2 were observed at a wavelength of 676 nm in many C_{60} -sensitized DCDHF glasses.^[11] These DCDHF glasses possess high electro-optic nonlinearity of $\Delta n \sim 0.01$ at an electric field of $30 \text{ V}/\mu\text{m}$ due to the high concentration of the nonlinear chromophore in the monolithic compound. In all DCDHF glasses, the ability of the chromophores to reorient in the electric field strongly depends on temperature relative to T_g . The orientational speed varies between $\sim 0.02 \text{ s}^{-1}$ at several degrees below T_g to $\sim 20 \text{ s}^{-1}$ at $\sim 15\text{-}20 \text{ }^\circ\text{C}$ above T_g .

In terms of PR performance, high PR two-beam coupling net gain coefficients of $\sim 200 \text{ cm}^{-1}$ at an electric field of $30 \text{ V}/\mu\text{m}$ were achieved in several glasses, sensitized with C_{60} , at a wavelength of 676 nm . Similar values at a wavelength of 830 nm were observed in a thiophene-containing **mix 5** sensitized with TNFM. At a wavelength of 676 nm and temperatures below T_g , the PR dynamics is orientationally-limited, with PR rise speed values of $\sim 0.02\text{-}0.05 \text{ s}^{-1}$. The PR speed is strongly dependent on temperature relative to T_g , and optimal PR performance is achieved at several degrees above T_g , with a PR speed reaching $\sim 1\text{-}2 \text{ s}^{-1}$. A detailed study of temperature dependence of all the parameters relevant for both steady-state and dynamic PR performance will be reported elsewhere.

Despite some excellent PR properties of DCDHF glasses, several issues are yet to be resolved. One of the issues important for using these materials in applications is thermal stability. Although there are several stable DCDHF glasses and mixtures, the best performing compounds are not necessarily among them. For example, our best performing compound in the near infrared wavelength region, **mix 5/TNFM**, is unstable. Another issue which is somewhat connected to thermal stability is the beam fanning effect. As high PR gain materials, DCDHF glasses exhibit strong beam fanning effect due to amplified scattering.^[10,11] However, the strength of this effect, which could be undesirable or desirable depending on application, strongly depends on the concentration of minute scattering centers in the material, which is related to thermodynamic stability of the phase. Therefore, in a thermally stable material with no nucleation centers, the beam fanning effect should be smaller. In contrast, scattering centers can be introduced in the material if the power loss due to fanning is desirable. Finally, for certain applications, temperature stabilization of the sample will be required to obtain well-defined dynamical performance.

ACKNOWLEDGEMENT

The authors gratefully acknowledge support of this work by AFOSR Grant No. F49620-00-1-0038.

REFERENCES

- [1] P. Yeh, *Introduction to Photorefractive Nonlinear Optics*, John Wiley, New York, 1993.
- [2] J. P. Huignard, P. Gunter, *Top. Appl. Phys.* **62**, 1, 1989.
- [3] L. Solymar, D. J. Webb, A. Grunnet-Jepsen, *The Physics and Applications of Photorefractive Materials*, Clarendon Press, Oxford, 1996.
- [4] W. E. Moerner, A. Grunnet-Jepsen, C. L. Thompson, *Annu. Rev. Mater. Sci.* **27**, 585, 1997.
- [5] A. Goonesekera, S. Ducharme, *J. Appl. Phys.* **85**, 6506, 1999.
- [6] F. Wurthner, S. Yao, *Angew. Chem.-Int. Edit.* **39**, 1978, 2000.

- [7] K. Meerholz, R. Bittner, Y. DeNardin, C. Brauchle, E. Hendrickx, B. L. Volodin, B. Kippelen, N. Peyghambarian, *Adv. Mater.* **9**, 1043, 1997.
- [8] E. Hendrickx, B. L. Volodin, D. D. Steele, J. L. Maldonado, J. F. Wang, B. Kippelen, N. Peyghambarian, *Appl. Phys. Lett.* **71**, 1159, 1997.
- [9] D. Wright, U. Gubler, Y. Roh, W. E. Moerner, M. He, R. J. Twieg, *Appl. Phys. Lett.* **79**, 4274, 2001.
- [10] U. Gubler, M. He, D. Wright, Y. Roh, R. Twieg, W. E. Moerner, *Adv. Mater.* **14**, 313, 2002.
- [11] O. Ostroverkhova, U. Gubler, D. Wright, W. E. Moerner, M. He, R. Twieg, *Adv. Fun. Mat. appearing in 2002*.
- [12] M. He, R. Twieg, O. Ostroverkhova, U. Gubler, D. Wright, W. E. Moerner, in *SPIE Proceedings*, Vol. 4802, Seattle, 2002
- [13] M. Kuzyk, in *Characterization Techniques and Tabulations for Organic Nonlinear Optical Materials*, Vol. 60 (Eds: M. Kuzyk, C. Dirk), Marcel Dekker, Inc., New York, 1998.
- [14] A. Grunnet-Jepsen, D. Wright, B. Smith, M. S. Bratcher, M. S. DeClue, J. S. Siegel, W. E. Moerner, *Chem. Phys. Lett.* **291**, 553, 1998.
- [15] D. Van Steenwinckel, E. Hendrickx, A. Persoons, *J. Chem. Phys.* **114**, 9557, 2001.
- [16] O. Ostroverkhova, K. D. Singer, *J. Appl. Phys.* **92**, 2002.
- [17] A. Grunnet-Jepsen, C. L. Thompson, W. E. Moerner, *J. Opt. Soc. Am. B* **15**, 905, 1998.